538 *Macromolecules* **2010**, *43*, 538–542
DOI: 10.1021/ma901845z

Macromolecules
ARTICLE

Liquid- to Solid-Like Failure Mechanism of Thin Polymer Films at Micro- and Nanoscales

Hongbo Zeng,*[,†,‡] Boxin Zhao,[‡,§] Jacob N. Israelachvili,*[,‡] and Matthew Tirrell[‡,⊥]

[†]*Department of Chemical and Materials Engineering, University of Alberta, Edmonton, Alberta, Canada, T6G 2 V4,* [‡]*Department of Chemical Engineering, and Materials Research Laboratory, University of California, Santa Barbara, California 93106,* [§]*Chemical Engineering Department, University of Waterloo, Ontario, Canada, and* [⊥]*Department of Bioengineering, Materials Science and Engineering, Chemical Engineering, University of California, Berkeley, California 94720*

Received August 19, 2009; Revised Manuscript Received October 28, 2009

ABSTRACT: A surface forces apparatus and various optical visualization techniques were used to study the transition mechanisms between liquid-like snapping and solid-like failure at nano- and microscales. Transient deformations and flows of polymer necks were studied over a large range of pulling forces, pulling rates, temperatures, and viscosities. A continuous transition is suggested—from simple neck-thinning and snapping, through viscous fingering, to sharp solid-like cracking— between these two limiting modes of failure if one chooses to vary the system properties and experimental conditions in a systematic way. The Saffman−Taylor fingering equation was found to remain valid down to nanoscopic dimensions, and a modified version of it is suggested to be suitable to elastic, solid-like materials.

Materials fail at very different length and time scales, from the macroscopic to the nanoscopic, and from μs to creeping failure over many years [note that polymer materials (melts) can encompass a very wide range of creep behavior]. The first scientific analysis of the failure of brittle materials by Griffith[1] was followed by experimental studies on the failure and deformations of soft adhesive layers (tack), and viscous and viscoelastic materials, and theoretical studies on crack initiation and propagation.[2−14] Failure of solids is commonly divided into brittle and ductile (plastic) failure, with different mechanisms and models applied to each. Failure of solid material arises both from bulk and surface properties, involving cracks, fingers, and internal cavities.[2−12,15−17]

The breakup or detachment of liquids is very different from the cracking of solids: a liquid column thins before snapping or breaks up into droplets (Rayleigh instability[18]). Liquid deformations are determined by surface tension and viscous forces, while those of solids by their elastic and tensile moduli. Nevertheless, one may ask: Is there a *fundamental* difference? Or: Is there a *gradual* or *continuous* transition between these two apparently very different failure mechanisms?

Using a surface forces apparatus (SFA) coupled to various optical visualization techniques,[11,18] we conducted both compression and tensile measurements of polymer bridges to investigate the transition between pure liquid-like and solid-like flow and failure. Some recent papers reported on SFA experiments of the transient deformations and flows during adhesion, coalescence and spreading of polymers and sugars over a range of rates and temperatures that spanned the liquid- to solid-like regimes as defined by the Deborah number *De*, being below or above 1, respectively.[1,15,16] Here, we focused on the transition when polymer bridges are subjected to tensile loading leading to failure.

Polystyrenes (PS) were chosen for our study: PS 590 (M_w = 590), $M_w/M_n \leqslant 1.1$, bulk shear viscosity $\eta \approx 230$ Pa s at 24.0 °C was purchased from Scientific Polymer Products Inc. PS 1300, $M_w/M_n \leqslant 1.1$, $T_g \approx 45$ °C, and PS 1390, $M_w/M_n \leqslant 1.06$, $T_g \approx 46$ °C were purchased from Pressure Chemical Co. The glass transition temperatures T_g were measured by differential scanning calorimetry (DSC) at a heating rate of 10 °C/min. Polymer films were prepared by spin-coating a droplet of PS−toluene solution on a mica substrate glued on silica disks, then very slowly drying under reduced pressure overnight (> 10 h) to remove the solvent and leave a film of uniform thickness, then mounted into the SFA chamber in the "crossed cylinders" geometry (each cylinder of radius R = 2 cm), which locally corresponds to a sphere of radius R on a flat surface or to two spheres each of radius 2R. The film thicknesses were measured *in situ* in the SFA using the FECO (fringes of equal chromatic order) optical interference technique, and were in the range T = 80−120 nm, and experiments were conducted between 24 and 51 °C. We have also studied polymers with high molecular weights such as polydimethylsiloxane (PDMS) melts with MW∼200 kDa, as well as small nonpolymeric molecular materials such as glucose.[19] Their fracture phenomena and mechanism are very similar to the polystyrenes shown in this study.

Figure 1A shows the experiment geometry, and Figure 1B shows top-view microscope images of inward fingering (of air) during the separation process of a PS 1300 neck of initial diameter $2r \approx 150\,\mu$m, $D \approx 100$ nm, at 51 °C (cf. T_g = 45 °C). The fingering patterns observed are typical of detaching PS necks in the molten state (discussed further below). In these experiments, the polymer-air interfaces were initially smooth and featureless, and remained so after the surfaces came into adhesive contact and instantaneously (within milliseconds) deformed elastically into a Johnson−Kendall−Roberts- (JKR-) like geometry.[20] The molecularly sharp JKR edge quickly becomes rounded (within seconds) due to the flow of the viscoelastic material to the boundary, driven by the very high Laplace pressure at the bifurcation region.[15,18] With time, if the surfaces are allowed to remain in contact, the contact radius continues to grow and the curvature at the edge continues to decrease (Figure 1A).

*Corresponding authors. E-mail: (J.N.I.) jacob@engineering.ucsb.edu; (H.Z.) hongbo.zeng@ualberta.ca.

 Published on Web 11/16/2009

On pulling the surfaces, depending on the rate, the neck narrows, but also develops rounded fingers that move inward faster than the decrease in the neck radius r. As the neck approaches the point of detachment (snapping) the advancing fingers accelerate and split into progressively smaller and sharper dendrites. The final stage of detachment is often preceded by the appearance of vapor or vacuum cavities in the film.

Defining the Deborah number De in terms of the shear strain rate during the detachment as $De = \tau(\partial r_{in}/\partial t)/D$, where τ is the shear relaxation time of the polymer (more information and values for τ are given in the Supporting Information), D is the gap distance, and $\partial r_{in}/\partial t$ is the velocity of the inner boundary of the fingers during separation, then the maximum Deborah number De_{max} will be given by eq 1:

$$De_{max} = \tau(\partial r_{in}/\partial t)_{max}/D \quad (1)$$

where $(\partial r_{in}/\partial t)_{max}$ is the velocity of the fastest moving finger during separation. Figure 1(C) shows the changes of the De_{max} *vs* D during the separation process. The minimum (critical) wavelengths λ_c of the fingers are also shown. The labels a−e in Figure 1C correspond to the images in Figure 1B. The (instantaneous) wavelength measured is the width (or diameter) of the fastest moving finger at a particular place and time. Please note that because of the complexity of the experimental geometry in this study shown in Figure 1a, the finger propagation velocity (or polymer-air interfacial velocity) is different at different locations and times, i.e., the finger wavelengths also change with time. This complex situation also arises because of the experimental conditions: we fixed the separation (or tensile) force rate during the separation, which is different from conventional probe-tack tests where the separation velocity is kept constant.

The changes in De_{max} during separations under four different driving separation velocities $V_\perp$ are shown in Figure S1, which all peak at $De_{max} > 1$. The faster the separation velocities, the larger the peak values of De_{max}.

Figure 2 shows typical top-view microscopic images of the separation of a PS 590 neck of initial diameter $2r \approx 200\ \mu$m, $D \approx$ 70 nm, at 24 °C. The two PS 590 films were first brought into contact, then kept in contact for 10 min under zero external load, and were then separated at $V_\perp = 0.5\ \mu$m/s ($K_\perp = 800$ N/m, $\therefore$ dF/d$t = K_\perp V_\perp = 0.4$ mN/s). The transition of the fracture process from smoothly rounded fingers to increasingly sharper "crack tips", as mentioned above, is clearly apparent here especially just before the two surfaces finally detach (Figure 2e).

Figure 3 also shows another type of separation of a PS 590 neck but for a smaller initial gap of $D = 40$ nm and higher dF/dt of 2.4 mN/s, where cavities were now observed: the large, single cavity at the center of the neck may be contrasted with the many small ones that appear throughout the neck (Figure 1e).

Under the conditions of Figure 3A, there are two regions of high De—one at the inwardly growing boundary (smooth or fingered) and the other at the tips of the outwardly growing cavity fingers. Figure 3B shows the progressive evolution of the two De_{max} values. It is notable that the highest De occurs at the explosive appearance (inception) of the central cavity, which grows out as highly pointed tips, i.e., as highly dendritic Saffman−Taylor fingers (see below) or microcracks. The cavity fingers then slow down, but are soon met by the inwardly *accelerating* fingers from the boundary, which causes the two De values to merge and increase again as the neck finally ruptures.

Fingering instabilities are commonly seen during adhesive debonding and failure of viscoelastic materials,[2,10,11] which

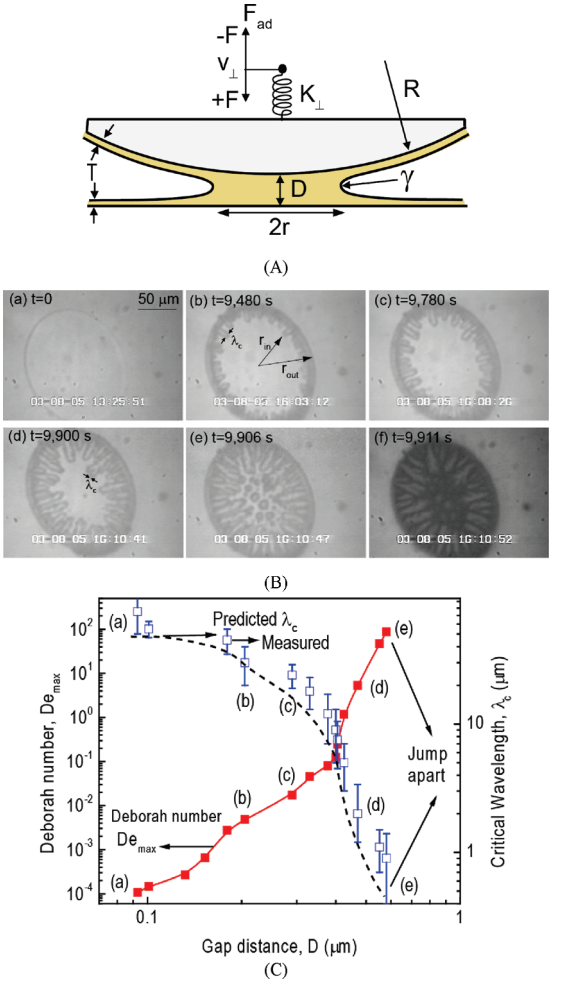

Figure 1. (A) Experimental contact geometry: T = initial (deposited) polymer film thickness on each mica surface, D = distance between mica surfaces measured during experiments, F = externally applied load, F_{ad} = pull-off (adhesion) force, R = radius of (undeformed) surfaces, $2r$ = diameter of contact neck, $K_\perp$ = spring constant of the normal force-measuring spring supporting the moving surface, and $V_\perp$ = external driving velocity of the spring. (B) (a−f) Top-view microscopic images of a thinning neck of PS 1300 at different times for $V_\perp \sim 17$ nm/s. (C) De_{max} and measured finger wavelength, and predicted λ_c by eq 2 (dashed curve) vs gap distance D during the separation of the two PS 1300 films shown in part B. Other experimental conditions: PS 1300 initial film thickness T = 80 nm, $K_\perp$ = 600 N/m, temperature = 51 °C; the two films were kept in contact under an external load of F = 30 mN for 1 h during which time they fully coalesced before the separation was commenced.

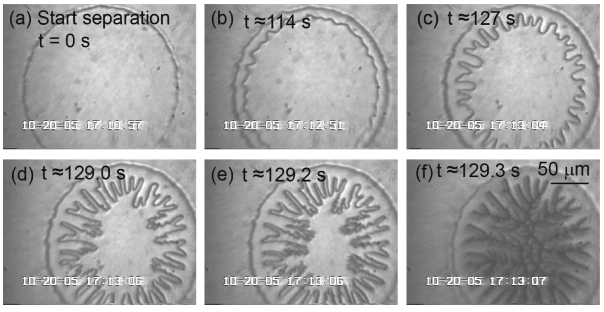

Figure 2. Top-view microscopic images during the separation of two PS 590 films, kept in contact for 10 min under zero external load $F = 0$ before separation at 24 °C; initial film thickness ~100 nm.

are normally described by the so-called Saffman-Taylor (ST) Fingering Instability[21,22] which predicts that fingers of

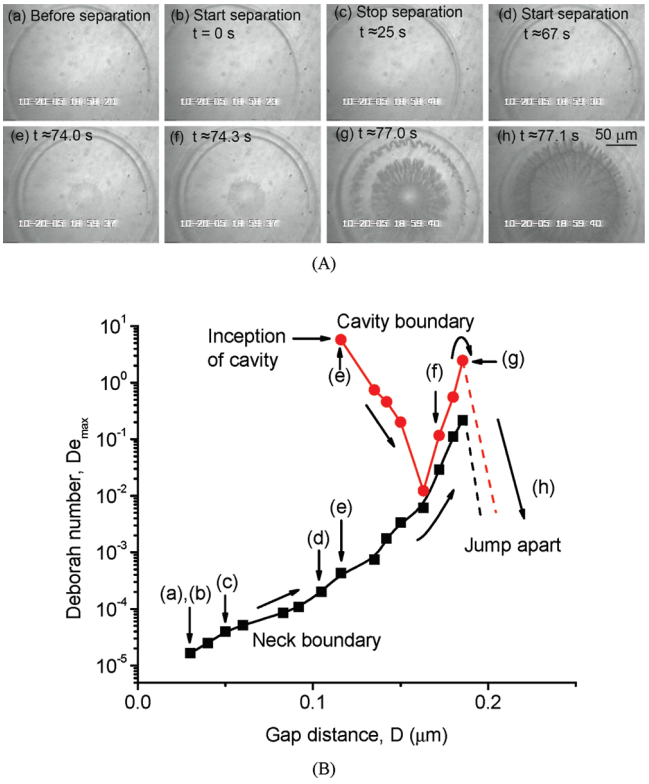

Figure 3. (A) Top-view microscopic images during the separation of two PS 590 films (kept in contact for 30 min under zero external load $F = 0$ before separation), first separated for 25 s, then waiting for 42 s, then separated again at a driving velocity of ~3 μm/s ($K_\perp = 800$ N/m, $dF/dt = K_\perp V_\perp = 2.4$ mN/s): after 7 s cavities appeared (e) and soon after the surfaces jumped apart (h). (B) De_{max} vs gap distance during the separation process shown in part A. Experimental temperature: 24 °C. Initial film thickness: $T \sim 100$ nm.

wavelength larger than λ_c will develop. λ_c is the critical or minimum finger wavelength given by eq 2

$$\lambda_c = 2\pi b\sqrt{\gamma/12V(\eta_1 - \eta_2)} \qquad (2)$$

$$= 2\pi b\sqrt{\gamma/12V\eta_1}(\eta_1 \gg \eta_2)$$

where V is the velocity of the interface, γ the interfacial tension,[21,23] b is the gap height, and η_i ($i = 1, 2$) are the shear viscosities of the two fluids (polymer and air in our study). For our geometry we may put $b \approx D$ and $V = dr/dt$. Note: eq 2 does not predict a single wavelength but the minimum wavelength. In our study, the wavelengths changed as the fingers moved from the periphery to the center, and varied with time, as did the fingering velocity. We used the wavelength of the fastest moving fingers to compare with the theoretical wavelengths using the instantaneous values of their velocities.

Most previous studies have focused on the ST fingering in films of thickness 0.01−1 mm, compared to our much thinner films of thickness ~100 nm.[8−11,24] However, the transition from rounded fingers to sharp crack-failure, especially in submicrometer geometries, has not been previously measured or theoretically analyzed. Sharp boundaries are predicted to arise in certain models of moving liquid boundaries,[22,25] but these assume zero surface tension of the fluid ($\gamma = 0$) which, according to the ST equation, predicts infinitely sharp fingers at *any* finite velocity V.

Figure 1C showed the measured wavelengths of the fingers λ *vs* gap distance D during the separation process as visualized in Figure 1B. The dashed curve is the calculated critical wavelength

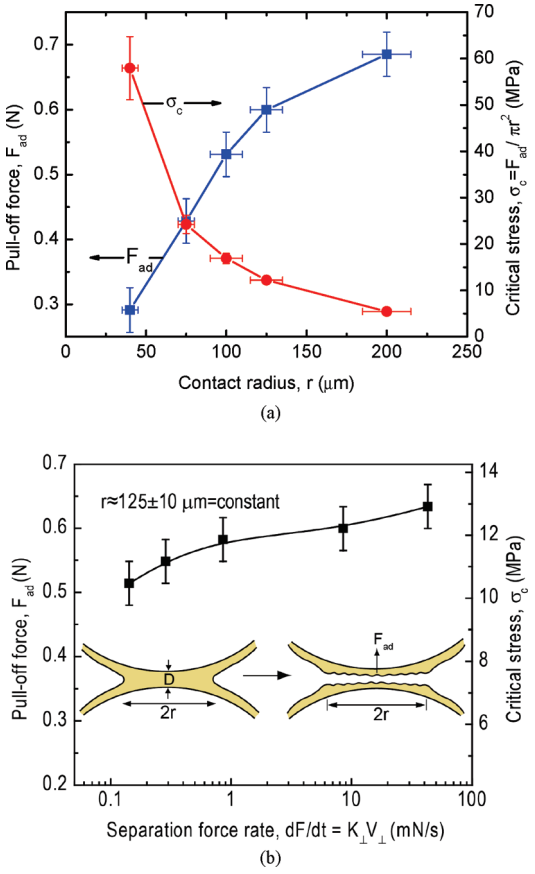

Figure 4. (a) Pull-off force F_{ad} and critical tensile stress $\sigma_c = F_{ad}/\pi r^2$ vs neck radius r during the detachment of a fully coalesced PS 1390 neck of thickness $T \sim 120$ nm at $dF/dt \approx 8.6$ mN/s. (b) F_{ad} and σ_c vs separation force rate $dF/dt = K_\perp V_\perp$, for a neck radius of $r = 125 \pm 10$ μm.

based on eq 2, which closely follows the experimental data. Figure 1C also shows how λ decreases as De increases, showing a minimum value when De peaks at $De_{max} \approx 90$.

We now report on our measurements of the separation of a polystyrene (PS 1390) neck in the glassy, rather than viscoelastic, state. In these experiments, the PS films in the SFA chamber were first heated to 30 °C above $T_g \approx 46$ °C. The molten films were then brought into contact, at which point they coalesced into a continuous neck which continued to grow with time. Once the desired neck radius r was reached, the whole system was rapidly frozen with liquid N_2. After the system had reached room temperature (24 °C), the two films were separated at different tensile force rates, dF/dt. Figure 4a shows the relationship between the measured pull-off (adhesion) forces, F_{ad}, and critical tensile stresses, $\sigma_c = F_{ad}/\pi r^2$, as a function of r. Each measurement was repeated at least three times. As shown in Figure 4a, F_{ad} increases while σ_c decreases as r increases. To our knowledge, there is no previous report of such an effect for tensile or fracture tests of polymer thin films. However, previous studies have found a similar effect for thin fibers and whiskers of metals, glasses and polymers,[26] where one of the major explanations is the reduction in the probability of defects (per unit area) with decreasing area: thus we expect the density of crack-initiating defects to be proportional to the circumference, or radius r, so that the probability of the presence of defects increases as r increases. This explanation also applies to the phenomenon observed here (Figure 4a). The effect of dF/dt on F_{ad} is shown in the semilog plot of Figure 4b where the pull off force/stress axis is the linear scale. The pull-off force and critical stress remain almost constant when pull-off rate changed by more than 3 orders of magnitude.

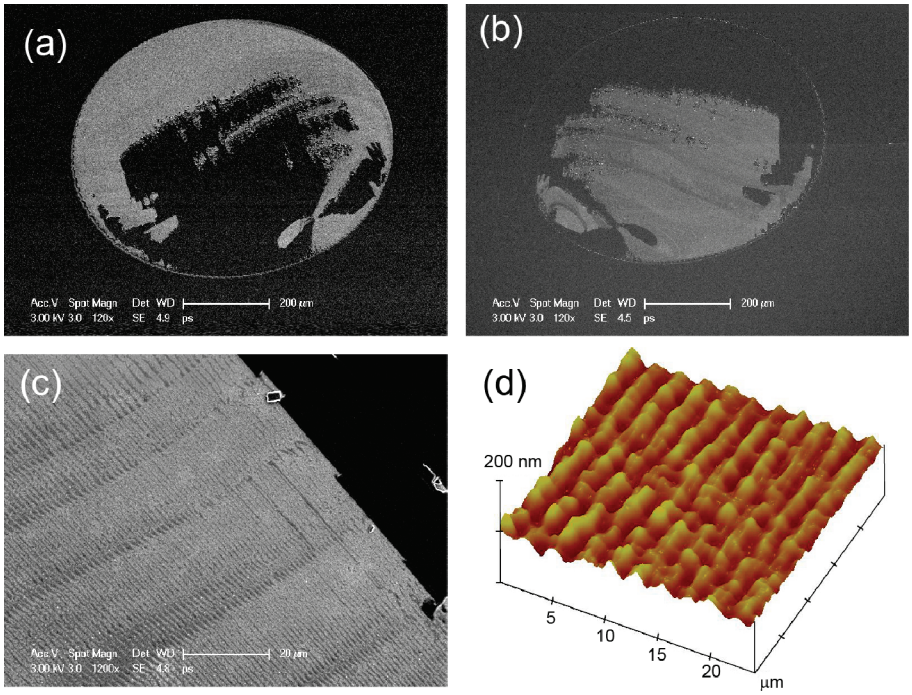

Figure 5. Typical SEM and AFM images of PS 1390 neck after fracture at 24 °C, of which parts a and b show complementary faces from the same neck after fracture.

Figures 5 and S2 show typical scanning electron microscope (SEM) images of two complementary surfaces of PS 1390 at $T < T_g$, i.e., in the glassy state, after they have fractured, and Figures 5d and S3 show higher resolution atomic force microscope (AFM) images of the fractured surfaces. Pease et al.[27] recently observed similar surface patterns when a thin glassy featureless film was confined between two rigid plates and the two plates were then "prised apart from an edge" causing fracture of the film, and they mainly focused at the surface structures. The SEM and AFM images reveal sharp cracks and linear, nearly parallel bands, which are in marked contrast to the radial fingers developed during the separation of the viscous liquids. The linear bands shown in Figure 5, S2 and S3 arise because once a nanocrack is initiated at the polymer−air interface, it moves very rapidly inward along a given (linear) direction—the crack front direction. Apparently, the rapid movement of this crack across the whole neck suppresses the propagation of other cracks.

To summarize, the transition from fluid-like to solid-like fracture (rounded radial fingers to sharp linear cracks) manifests itself both visually and quantitatively. First, with increasing interface velocity V, the interface becomes rippled (fingered), then the tips of the fingers become progressively smaller as they turn into sharply pointed crack tips. Second, the radial ripples or fingers become linear cracks or grooves. Third, the transition is correlated with the Deborah number De: when $De > 1$ the fluid is being sheared faster than its ability to relax (its characteristic relaxation time) and responds more like a solid.

Quantitatively, assuming that eq 2 remains valid even at the nanoscale, inputting some typical experimental values: $\gamma \approx 0.033$ J/m^2, $b \approx 100-500$ nm, $\Delta\eta \approx 10^2-10^5$ Pa s, and with V in the range 0.0001−500 μm/s during a separation, the predicted wavelength of the fingers decreases from $\lambda > 10\ \mu$m at $De_{max} \ll 1$ (e.g., $b = 100$ nm, $V = 0.001\ \mu$m/s, $\Delta\eta \approx 230$ Pa s, then $\lambda_c = 68.7\ \mu$m, and $De_{max} \approx 10^{-5}$) to $\lambda < 0.1\ \mu$m at $De_{max} > 1$ (e.g., $b = 500$ nm, $V = 100\ \mu$m/s, $\Delta\eta \approx 10^5$ Pa s, then $\lambda_c = 0.052\ \mu$m, and $De_{max} \approx 90$), which is consistent with the experimentally observed values in Figures 1,2,3, and 5.

For glassy polymers whose viscosities can be as high as 10^9 Pa s, the predicted wavelengths of crack tips fall in the range 0.3−1 nm, which brings it down to molecular dimensions. This estimate is consistent with the early experimental studies by Donald and Kramer[28] and Brown and Kramer[29] who used TEM and SAXS to show that the sizes of craze tips (or ultra narrow necks) in the crack zone of fractured glassy polymer films are about 10 nm. The above analysis suggests that the ST formalism may be valid not only for the separation of viscous liquids, but also for materials undergoing solid-like failure. Donald and Kramer[28] suggested a similar applicability of the ST equation at nanoscopic dimensions.

One should note that the above results and analysis focus on the cohesive failure of viscous or viscoelastic materials. In contrast, studies by Creton et al.[24] on the adhesive failure of elastic materials (fully cross-linked PDMS films), found that the fingering wavelengths are proportional to the film thickness T but independent of the pulling velocity of the punch.[6,24] Ghatak et al.[30] reached a similar conclusion in their peeling experiments of elastic adhesive tapes, which was subsequently analyzed theoretically by Adda-Bedia and Mahadevan.[12] These studies therefore suggested that the fracture mechanisms for viscous liquids and elastic solids are "distinct", i.e., fundamentally different.

There are three important issues to consider: (i) how the velocity V is defined in different types of experiments, (ii) whether the crack-tip moves at a constant velocity or in stick−slip jumps, and (iii) whether or how the Saffman−Taylor equation may be applied to elastic solids or when ηV becomes very large.

(i) In the above-mentioned punch-pulling experiments[24] the velocity was the *pulling* velocity, i.e., normal to the cracking film, rather than the crack-tip or fingering velocity in the plane of the film. These two velocities are quite different and depend on different system parameters: for elastic materials the fingering/crack tip velocities are limiting velocities (like the speed of sound through a material) which depend on the intrinsic properties of the film material as well as on the film geometry such as its thickness at the time the fingers or cracks propagate (this issue is discussed more fully in the next paragraph). (ii) Cracks often

propagate by stick−slip motion, leaving micrometer-sized terraces as shown in Figure 5c. In such cases, the mean, macroscopically measured, crack velocity will be quite different from the real (slip) velocity which would be much faster. (iii) By definition, viscosity η = shear stress/shear rate = $\sigma/(V/b)$; thus, eq 2 can be rewritten as

$$\lambda_c = 2\pi\sqrt{\frac{\gamma}{12(\sigma/b)}} \tag{3a}$$

$$= 2\pi b\sqrt{\frac{\gamma}{12\sigma b}} \propto b\sqrt{\frac{\gamma}{\sigma b}} \tag{3b}$$

where we see that the wavelength can also be considered to be determined by a balance between the surface energy γ, and the pressure gradient at the interface σ/b. Equation 3b does not contain the viscosity η and provides a more general and nonfluid dynamics view of the failure of more solid-like materials[8] where the limiting finger wavelength depends on the surface tension γ, yield strength σ and film thickness b. For elastic films $\gamma \sim G_c$ and $\sigma \sim E$, where G_c is the critical energy release rate and E is the elastic modulus of the polymer films.[31,32] Thus, $\gamma/\sigma b \sim G_c/Eb$, which is independent of the crack velocity or pulling velocity V. In this limit, therefore, we expect the limiting wavelength of the fingers (the crack tip radius) to be proportional to the film thickness b and independent of V.[33] This analysis is consistent with the recent experimental results on the failure of elastic and fully cross-linked PDMS films (where the smallest fingering wavelength was about 100 μm).[24] In contrast, for the viscous and viscoelastic necks studied here, the Saffman−Taylor equation appears to remain valid down to fingering wavelengths (crack-tip radii) having submicroscopic to nanoscopic dimensions, as previously also noted by others.[28,29]

Our study suggests that one can go continuously from one regime, limit or mechanism (of viscous liquid-like failure) to the other (of elastic solid-like fracture) if one chooses to vary the system properties and experimental conditions in a systematic way. The Saffman−Taylor fingering mechanism, eq 2, and its analogue for more solid-like materials ($De \gg 1$, high ηV) eq 33, remains valid over the whole range.

Acknowledgment. This work was supported by DOE Grant DE-FG02-87ER45331. The authors thank Professor Edward J. Kramer and Professor George M. Homsy for helpful discussions.

Supporting Information Available: Figures showing the driving velocity effects on the separation process and more SEM and AFM images of fractured polymer surfaces and text discussing the relaxation time information on the polymers used. This material is available free of charge via the Internet at http://pubs.acs.org.

References and Notes

(1) Johnson, K. L. *Contact mechanics*; Cambridge University Press: Cambridge, U.K., and New York, 1985.
(2) Fields, R. J.; Ashby, M. F. *Philos. Mag.* **1976**, *33*, 33–48.
(3) Creton, C.; Kramer, E. J.; Hui, C. Y.; Brown, H. R. *Macromolecules* **1992**, *25*, 3075–3088.
(4) Gay, C.; Leibler, L. *Phys. Rev. Lett.* **1999**, *82*, 936–939.
(5) Crosby, A. J.; Shull, K. R.; Lakrout, H.; Creton, C. *J. Appl. Phys.* **2000**, *88*, 2956–2966.
(6) Shull, K. R.; Flanigan, C. M.; Crosby, A. J. *Phys. Rev. Lett.* **2000**, *84*, 3057–3060.
(7) McKinley, G. H.; Sridhar, T. *Annu. Rev. Fluid Mech.* **2002**, *34*, 375–415.
(8) Derks, D.; Lindner, A.; Creton, C.; Bonn, D. *J. Appl. Phys.* **2003**, *93*, 1557–1566.
(9) Poivet, S.; Nallet, F.; Gay, C.; Fabre, P. *Europhys. Lett.* **2003**, *62*, 244–250.
(10) Shull, K. R.; Creton, C. *J. Polym. Sci., Part B: Polym. Phys.* **2004**, *42*, 4023–4043.
(11) Zeng, H. B.; Maeda, N.; Chen, N. H.; Tirrell, M.; Israelachvili, J. *Macromolecules* **2006**, *39*, 2350–2363.
(12) Adda-Bedia, M.; Mahadevan, L. *Proc. R. Soc. A: Math. Phys. Eng. Sci.* **2006**, *462*, 3233–3251.
(13) Horn, R. G.; Israelachvili, J. N.; Pribac, F. *J. Colloid Interface Sci.* **1987**, *115*, 480–492.
(14) Bhushan, B. *Nanotribology and nanomechanics: an introduction*, 2nd ed.; Springer: Berlin, 2008.
(15) Zeng, H.; Tian, Y.; Zhao, B.; Tirrell, M.; Israelachvili, J. *Macromolecules* **2007**, *40*, 8409–8422.
(16) Zeng, H. B.; Zhao, B. X.; Tian, Y.; Tirrell, M.; Leal, L. G.; Israelachvili, J. N. *Soft Matter* **2007**, *3*, 88–93.
(17) Persson, B. N. J. *Surf. Sci. Rep.* **2006**, *61*, 201–227.
(18) Israelachvili, J. N. *Intermolecular and surface forces*; 2nd ed.; Academic Press: Amsterdam ; Boston, 1992.
(19) Zhao, B. X.; Zeng, H. B.; Tian, Y.; Israelachvili, J. *Proc. Natl. Acad. Sci. U.S.A.* **2006**, *103*, 19624–19629.
(20) Johnson, K. L.; Kendall, K.; Roberts, A. D. *Proc. R. Soc. London Ser. A: Math. Phys. Sci.* **1971**, *324*, 301.
(21) Saffman, P. G.; Taylor, G. *Proc. R. Soc. London Ser. A: Math. Phys. Sci.* **1958**, *245*, 312.
(22) Homsy, G. M. *Annu. Rev. Fluid Mech.* **1987**, *19*, 271–311.
(23) Chuoke, R. L.; Vanmeurs, P.; Vanderpoel, C. *Trans. Am. Inst. Mining Metall. Eng.* **1959**, *216*, 188–194.
(24) Nase, J.; Lindner, A.; Creton, C. *Phys. Rev. Lett.* **2008**, 101.
(25) Ceniceros, H. D.; Hou, T. Y.; Si, H. *Phys. Fluids* **1999**, *11*, 2471–2486.
(26) Vasiliev, V. Z.; Kaptelin, S. Y. *J. Appl. Mech. Tech. Phys.* **1992**, *33*, 598–602.
(27) Pease, L. F.; Deshpande, P.; Wang, Y.; Russel, W. B.; Chou, S. Y. *Nat. Nanotechnol.* **2007**, *2*, 545–548.
(28) Donald, A. M.; Kramer, E. J. *Philos. Mag. A: Phys. Condens. Matter Struct. Defects Mech. Properties* **1981**, *43*, 857–870.
(29) Brown, H. R.; Kramer, E. J. *J. Macromol. Sci.—Phys.* **1981**, *B19*, 487–522.
(30) Ghatak, A.; Chaudhury, M. K.; Shenoy, V.; Sharma, A. *Phys. Rev. Lett.* **2000**, *85*, 4329–4332.
(31) McCrum, N. G.; Buckley, C. P.; Bucknall, C. B. *Principles of polymer engineering*, 2nd ed.; Oxford University Press: Oxford, U.K., and New York, 1997.
(32) Tabor, D. *Gases, liquids, and solids: and other states of matter*, 3rd ed.; Cambridge University Press: Cambridge, England, and New York, 1991.
(33) Strictly speaking, G_c is not a constant but is dependent on the cross-linking density ρ according to $G_c \propto a^{1/2}$, where a is the spacing between cross-links. Since $\rho \propto 1/a^3$, we therefore have $\sqrt{G_c} \propto 1/\rho^{1/12}$. Thus, we expect a very weak dependence of λ_c on ρ, which could easily be missed in experiments where ρ is varied by only a small amount. For example, in Figure 6 of Nase et al.[24] ρ was varied by a factor of 4 (from 1.5 to 6%). The results show a linear dependence of λ_c on b. The above analysis suggests a deviation of 12% from a linear dependence, which is within the experimental error.